



Feasibility of observing dayside aurora using NIR camera onboard high-altitude balloons

X.-Y. Zhou,¹ D. Lummerzheim,² R. Gladstone,³ and S. Gunapala¹

Received 28 October 2006; revised 19 December 2006; accepted 3 January 2007; published 8 February 2007.

[1] This letter reports a feasibility study on dayside auroral observation using a near-infrared (NIR) InGaAs camera from high-altitude, long-duration balloons. This effort is motivated by science interest in the dayside aurora. Model predictions indicate daytime observations are possible because the sky brightness significantly decreases towards longer wavelengths at certain altitude in the upper atmosphere, and the NIR ambient sky brightness substantially decreases with increasing altitude. To address the question whether aurora can indeed be detected in the upper atmosphere, auroral test observations were conducted at the Poker Flat Research Range from March 22 to April 26, 2005. The InGaAs camera used in this test covers a waveband from 900 to 1700 nm with a 320×256 focal plane array, $30 \times 30 \mu\text{m}$ pixels, and a 9° field of view. For one evening event, we estimate the NIR sky brightness using the MODTRAN atmospheric radiance model and compare it with the expected sky brightness at 30–50 km altitudes. The comparison indicates that the N_2^+ Meinel emission at ~ 1100 nm should be seen at 35–40 km altitudes and above, and therefore, confirms that such dayside auroral observations are feasible. Auroral studies using this method include, e.g., studies of interplanetary shock and pressure pulse induced auroras as well as conjugate auroras. **Citation:** Zhou, X.-Y., D. Lummerzheim, R. Gladstone, and S. Gunapala (2007), Feasibility of observing dayside aurora using NIR camera onboard high-altitude balloons, *Geophys. Res. Lett.*, 34, L03105, doi:10.1029/2006GL028611.

1. Introduction

[2] Along with many important nightside discoveries resulting from space-based observations, important dayside auroral phenomena and global auroral dynamics were unveiled by space-borne UV imagers [Craven *et al.*, 1986; Spann *et al.*, 1998; Zhou and Tsurutani, 1999; Hubert *et al.*, 2003], but at the expense of missing auroral microstructures. However, those structures are key to understand auroral particle acceleration. In addition, a long-time open question is whether auroral behavior differs in the sunlit ionosphere (where the conductivity is higher) from that in darkness. Therefore, efforts of closely observing dayside auroras have been attempted on several occasions, using other methods.

[3] In the late 1990s, new technologies for daytime airglow and auroral observations from the ground started to emerge [Chakrabarti, 1998]. One of the interesting results of their applications is the airglow observation from the Hi-TIES (High-Throughput Imaging Echelle Spectrograph) using the technology of diffuse imaging spectroscopy. The instrument used a mosaic of filters at the image plane, which is particularly advantageous for high resolution diffuse emission studies. The instrument was used to obtain the sky spectrum in a spectral region around 630 nm in twilight at 17:45 LT. Then, the airglow emission feature at 630.03 nm was given by the difference between the solar spectrum and sky spectrum. Pallamraju *et al.* [2004] have used a high-spectral-resolution imaging spectrograph, which is a direct descendant of Chakrabarti's Hi-TIES, to obtain meridional profiles of OI (630 nm) emission intensity from Sondrestrom with solar zenith angles from 87° to 93° . These profiles present the auroral emission at 630 nm only when the aurora is very intense compared to the background contribution from Rayleigh scattered sunlight. This technique provides profiles of auroral intensity at a given meridian, but is not easily extended into auroral imaging. Rees *et al.* [2000] used an imaging optical spectrometer based on two capacitance-stabilized Fabry-Perot etalons to obtain near-daytime auroral images of OI (630 nm) from Kiruna. Their instrument had a field of view (FOV) of about 90° . The obtained images were taken at dusk when the imager was zenith looking with a solar depression angle of 1.5° . While Rees *et al.* built up a complete two-dimensional image of the sky at 630 nm, they sacrificed both spatial and temporal resolution in the process of separating the auroral emission from the scattered sunlight. The OI (630 nm) emission originates from a forbidden transition and is thus long-lived. Even with higher spatial and temporal resolution imaging, the auroral structure that can be observed with this emission suffers from lack of spatial resolution and cannot provide high definition images of transient auroral emission features.

[4] Dayside auroral observation from the ground has been very challenging due to Rayleigh-scattered sunlight as well as the very limited locations from where the dayside aurora can be observed. However, a solution emerged when a NASA balloon successfully flew up to ~ 50 km altitude with ~ 700 kg suspended weight for more than 20 hours in 2002 (see NASA press release available at <http://www.gsfc.nasa.gov/news-release/releases/2002/h02-163.htm>). This new high-altitude balloon technology presents the opportunity to conduct dayside and conjugate auroral observations from near-infrared (NIR) imaging. In this paper, we describe how an InGaAs NIR camera may be used to overcome the sky brightness at balloon-accessible altitudes

¹Jet Propulsion Laboratory, Pasadena, California, USA.

²Geophysical Institute, University of Alaska at Fairbanks, Fairbanks, Alaska, USA.

³Southwest Research Institute, San Antonio, Texas, USA.

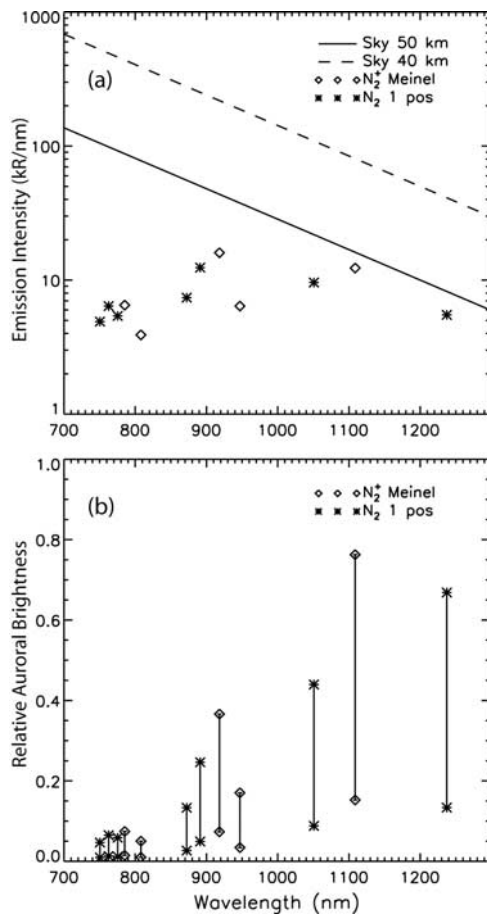


Figure 1. Near-infrared auroral brightness. (a) Comparison to the upper atmospheric sky intensity. (b) Relative auroral brightness for an assumed 10 mW m^{-2} energy flux.

and measure auroral N_2^+ Meinel emissions ($\sim 1100 \text{ nm}$ wavelength). Our test observations confirmed that the new approach is feasible.

2. New Method: The Principle

[5] Atmospheric modeling shows that the sky brightness (mainly Rayleigh scattered sunlight) decreases towards the longer wavelengths [e.g., Liou, 2002]. One such model is MODTRAN, which stands for MODerate spectral resolution atmospheric TRANSmittance [Anderson et al., 1999]. The model calculates atmospheric transmittance and radiance for a given altitude and viewing conditions. Figure 1 shows that at altitudes of 40–50 km, the sky intensity at near-infrared wavelengths becomes comparable to typical auroral intensity of N_2 emissions, especially the N_2^+ Meinel emission at 1109 nm. In Figure 1a, the oblique lines present the calculated sky intensity obtained from the MODTRAN model for a local zenith angle of $\text{LZA} = 80^\circ$, a local azimuthal angle (relative to the azimuth of the Sun) of $\text{LAZ} = 180^\circ$, and a solar zenith angle of $\text{SZA} = 90^\circ$. The N_2^+ Meinel brightness was calculated using Frank-Condon factors and relative auroral emissions from Vallance Jones [1974]. The relative auroral brightness (i.e., auroral inten-

sity/sky intensity) is shown in Figure 1b, which is obtained for an assumed auroral energy flux of 10 mW m^{-2} , representing moderate auroral brightness at nighttime. For each vertical segment, the top mark corresponds to the intensity ratio at 50 km altitude, the bottom to the intensity ratio at 40 km altitude. For the N_2^+ Meinel line at 1109 nm, the ratio increases from ~ 0.15 to 0.75 as the altitude increases from 40 to 50 km. It should be noted that in general when the auroral signal over background ratio is ~ 0.1 or higher, the aurora is detectable.

[6] The above results indicate that the N_2^+ Meinel auroral emission can very likely be seen, using a NIR camera above 40 km altitude. An excellent platform for such observations is a high-altitude, long-duration balloon, available with current NASA balloon technology.

3. Instrumentation

[7] One such NIR imaging technique uses an InGaAs (Indium Gallium Arsenide) camera developed at JPL. This InGaAs camera covers a waveband from 900 to 1700 nm and has a very low $1/f$ noise, high quantum efficiency, high operability, and uniformity [Bandara et al., 2004]. The camera has a small size of $10 \times 10 \times 20 \text{ cm}$, low mass of 2.5 kg, and low power consumption of 5.5 W. Those are significant advantages for high-altitude balloon missions.

[8] The camera has a 320×256 focal plane array (FPA), $30 \times 30 \mu\text{m}$ pixel size and 9° FOV. The high performance FPA hybrid is composed of a back-illuminated InGaAs detector (using Positive-Intrinsic-Negative photodiode pixels, which in principle can produce many spectral images per data cube). Two major advancements have contributed to the development of these FPAs: (1) an improvement in the read out integrated circuit (ROIC) design and (2) the higher quality 2D InGaAs PIN photodiodes. The ROIC is a capacitive transimpedance amplifier that can be switched from a low gain to a high gain. The spectral response of the InGaAs FPA is shown in Figure 2. For wavelengths 1100–1650 nm, the responsivity is above 0.5 (A/W), and the quantum efficiency exceeds 60%. The InGaAs FPA utilizes a low power ROIC that works in extremely low light levels. To enable higher resolution measurements, a larger format (such as 1024×1024 pixels) version of this type of ROIC

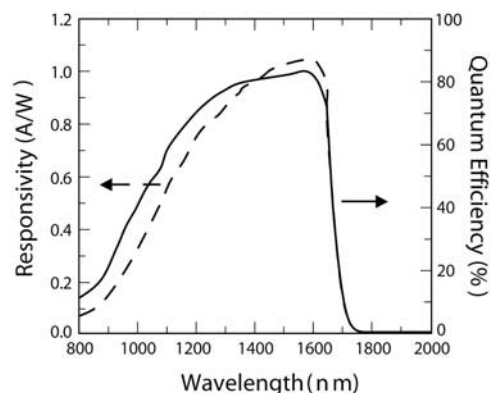


Figure 2. Responsivity (dashed line) and quantum efficiency (solid line) of an $\text{In}_{0.53}\text{Ga}_{0.47}\text{As}$ PIN photodiode at 296 K temperature.

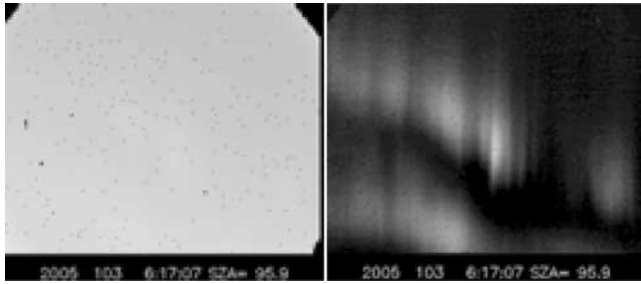


Figure 3. Comparison of two images (left) with and (right) without background. The image was taken at 2116:07 LT in evening twilight on April 13, 2005. The Sun was $\sim 6^\circ$ below the horizon (i.e., $\text{SZA} \approx 96^\circ$).

with smaller pixel size would be desirable for future balloon observations.

4. Test Observation Result

[9] As a proof of the concept for dayside auroral observations from balloon altitudes, we have conducted auroral test observations using the InGaAs NIR camera described in section 3. The camera was set up at the Poker Flat Research Range, during March 22–April 26, 2005. The camera pointed towards north and $\sim 30^\circ$ above the horizon. The NIR camera took one image per second. Good auroral images were obtained during nights, evening and morning twilight. Figure 3 shows a raw image (left) and the image after background removal (right). The background is obtained by averaging images over 40 seconds centered at the time of the image. All stars are removed as well. The dots visible in the image on the left are from bad pixels. In the raw image the aurora is almost not noticeable against the bright background. The sky background intensity is ~ 800 counts; the auroral intensity is ~ 50 – 70 counts above the background. It should be noted that this sky intensity includes the OH airglow around 1200–1700 nm and the twilight at 2116 LT. The OH airglow intensity is estimated

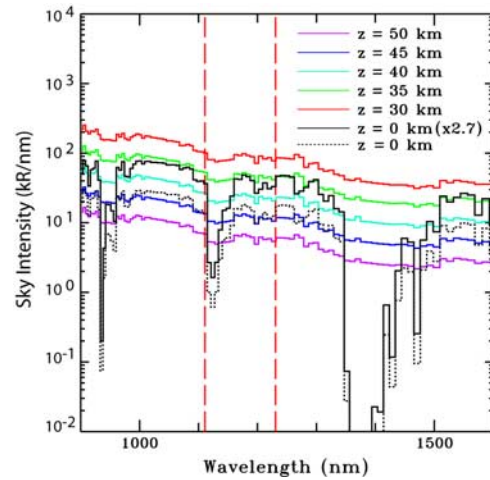


Figure 5. Comparison of sky intensity. On the ground (i.e., when $z = 0$ km), we used $\text{LZA} = 60^\circ$, $\text{LAZ} = 90^\circ$, and $\text{SZA} = 96^\circ$, which correspond to the conditions of the auroral observation shown in Figure 4. For $z = 30$ km and above, $\text{SZA} = 55^\circ$. The dotted line at $z = 0$ km is the sky intensity without OH airglow contribution. The solid black line at $z = 0$ km is the sky intensity including OH airglow contribution.

from the midnight sky intensity to be ~ 500 counts (we assumed that the OH airglow intensity does not change from 21 to 00 LT). This number is consistent with the work of *Remick et al.* [2001], i.e., the brightest OH airglow near 1500 nm is ~ 8 times brighter than the N_2^+ Meinel emission. Therefore, we estimate the twilight sky intensity contributes ~ 300 counts at 2116 LT, and, therefore, the OH airglow is 1.7 times brighter than the twilight sky at that time. Figure 4 shows an abrupt auroral morphology change within 10 sec observed during the evening twilight on April 13, 2005. An auroral arc was moving further north while becoming brighter and then began dimming away. Figure 4 demonstrates that after the background removal, we can see a lot of

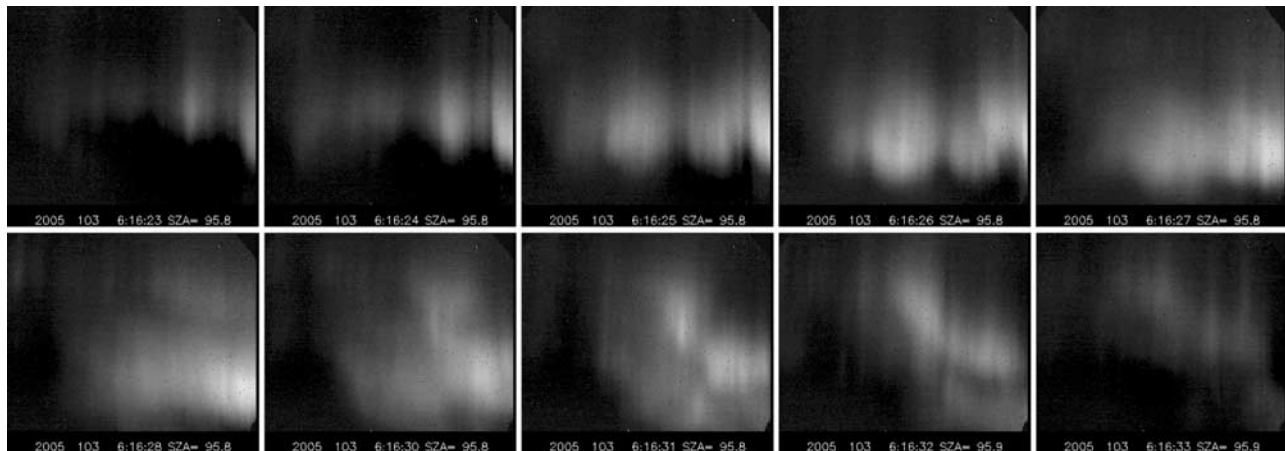


Figure 4. Auroras detected by the InGaAs NIR camera. The images were taken in evening twilight from 2116:23 to 2116:33 LT on April 13, 2005. Images are shown in one second cadence chronologically from left to right, then down to the second row. The SZA is $\approx 96^\circ$. Each image has had a background subtracted that was calculated from 40 images around the time of the image.

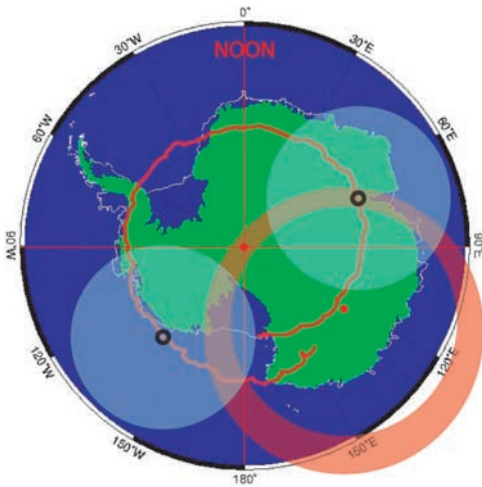


Figure 6. An example of auroral observation from balloons. See text for detailed explanation.

structure, and much dimmer aurora as well. More discussions about the intensity of the aurora, twilight and OH airglow as well as the method of the background subtraction can be found in *Zhou et al.* [2007].

[10] Figure 5 shows a comparison of sky intensity obtained from MODTRAN for different altitudes. Colored lines show the sky intensity from 30 to 50 km altitude in a wavelength range from 900 to 1600 nm, where the InGaAs camera has the best responsivity (see Figure 2). The black lines (both solid and dotted lines) are the sky intensity on the ground at the time when the observations shown in Figures 3 and 4 were conducted. Along the black lines, three large dips around ~ 950 , 1130, and 1400 nm are due to the tropospheric absorption. The two red vertical dashed lines indicate the N_2^+ Meinel line at 1109 nm and the N_2 first positive line at 1236 nm, which are the main contributors to the aurora seen in Figures 3 and 4. We have used $LZA = 60^\circ$ and $LAZ = 90^\circ$ for all altitudes. For altitudes of 30 km and higher, $SZA = 55^\circ$, which corresponds to the smallest solar zenith angle that would be observed by balloon during Antarctic summer (i.e., the highest elevation of the Sun above the horizon). For $z = 0$ km on the ground, $SZA = 96^\circ$, which indicates the Sun was 6° below the horizon at ~ 0616 UT at Poker Flat. The dotted black line is MODTRAN output that does not include the OH airglow. The solid black line is the one included the OH airglow contribution. The solid black line is obtained by increasing the MODTRAN prediction by a factor of 2.7 (when the ~ 1500 nm OH airglow is eliminated using a narrow band-pass filter). This correction is reasonable since the 500-count OH airglow contribution will not change, regardless of wavelength. The camera responsivity (see Figure 2) only affects the measured auroral intensity because the InGaAs detector is a bit more sensitive towards longer wavelengths, but not to the total OH airglow contribution because that is an integrated result. The comparison in Figure 5 indicates that the sky intensity in which the aurora was detected (see Figures 3

and 4) is similar to the sky up to 35–40 km altitude at the two wavelengths.

5. Auroral Observations From Balloon

[11] Most long-duration balloon flights have been conducted in Antarctica. The expected FOV coverage of an all-sky NIR InGaAs camera on a McMurdo-launched balloon is depicted in Figure 6. The red dot at the center is the geographic pole and the one in the lower right quadrant is the magnetic pole. The red wiggling curve is the trajectory of the MAXIS balloon mission in 2000 [*Millan et al.*, 2002]. The shaded red ring is a potential auroral oval at a moment when 0° geographic longitude is at local noon. Two small black circles are two possible balloon positions, and the lighter shaded circles represent the observable region for a camera at 40 km and an aurora at 200 km altitude. The trajectory can be 5° to 10° latitude smaller or larger. Flying one circle along a trajectory like this would take ~ 20 days, during which time the auroral oval continuously changes its orientation. As a result, the camera would sometimes see dayside aurora, nightside aurora, aurora at lower latitudes below the oval, or aurora at higher latitudes in the cap.

[12] Due to the limited land area of Antarctica, the major portion of the southern auroral oval is usually located above the ocean. Therefore, the ground-based auroral observation at the south pole is very constrained, especially for nightside observations. Auroral observations from balloons can partially remove this limitation.

6. Conclusion

[13] In this letter, we have studied the feasibility of balloon-borne dayside auroral observations. The result of test observations has confirmed that the dayside aurora should be seen at and above altitudes of 35–40 km. With current NASA balloon technology, flying at these altitudes with a 1000 kg payload is routine. Driven by the Antarctic circumpolar winds, a balloon can maintain a trajectory around the geographic pole over several weeks. Examples of such missions are available at <http://www.nsbfnasa.gov/index.html>.

[14] Auroral observation from balloons provides a unique opportunity for studying dayside auroral microstructures that is not possible from space-based observations and very difficult to do from the ground-based observation. The important auroral phenomena that can be studied via balloon observation include dayside aurora [*Sandholt et al.*, 2002], nightside aurora, shock aurora [*Zhou and Tsurutani*, 1999; *Zhou et al.*, 2003], cusp aurora, polar cap aurora, sub-latitude dayside and nightside aurora [*Liou et al.*, 2002; *Zhang et al.*, 2005], conjugate aurora, as well as extremely high-altitude aurora [*Mizuno et al.*, 2005]. Detailed discussions about the camera system development and the science applications of this new approach can be found in the work of *Zhou et al.* [2007].

[15] **Acknowledgments.** Portions of this research were performed at the Jet Propulsion Laboratory, California Institute of Technology, Pasadena, under contract with NASA. We appreciate J. Trinh for his work during the auroral test observations. We thank the Poker Flat Research Range for providing observation space and the Geophysical Institute at UAF for

additional support. Xiaoyan Zhou thanks D. Sibeck for his very helpful discussions.

References

- Anderson, G. P., et al. (1999), MODTRAN4: Radiative transfer modeling for remote sensing, *Proc. SPIE Int. Soc. Opt. Eng.*, 3666, 2–10.
- Bandara, S. V., et al. (2004), Multiband infrared detectors based on III-V materials, *Proc. SPIE Int. Soc. Opt. Eng.*, 5543, 1–8.
- Chakrabarti, S. (1998), Ground based spectroscopic studies of sunlit air-glow and aurora, *J. Atmos. Sol. Terr. Phys.*, 60, 1403–1423.
- Craven, J. D., L. A. Frank, C. T. Russell, E. E. Smith, and R. P. Lepping (1986), Global auroral responses to magnetospheric compressions by shocks in the solar wind: Two case studies, in *Solar Wind-Magnetosphere Coupling*, edited by Y. Kamide and J. A. Slavin, pp. 367–380, Terra Sci., Tokyo.
- Hubert, B., J. C. Gérard, S. A. Fuselier, and S. B. Mende (2003), Observation of dayside subauroral proton flashes with the IMAGE-FUV imagers, *Geophys. Res. Lett.*, 30(3), 1145, doi:10.1029/2002GL016464.
- Liou, K. N. (2002), *An Introduction to Atmospheric Radiation*, Elsevier, New York.
- Liou, K., C.-C. Wu, R. P. Lepping, P. T. Newell, and C.-I. Meng (2002), Midday sub-auroral patches (MSPs) associated with interplanetary shocks, *Geophys. Res. Lett.*, 29(16), 1771, doi:10.1029/2001GL014182.
- Millan, R. M., R. P. Lin, D. M. Smith, K. R. Lorentzen, and M. P. McCarthy (2002), X-ray observations of MeV electron precipitation with a balloon-borne germanium spectrometer, *Geophys. Res. Lett.*, 29(24), 2194, doi:10.1029/2002GL015922.
- Mizuno, D. R., et al. (2005), Very high altitude aurora observations with the Solar Mass Ejection Imager, *J. Geophys. Res.*, 110, A07230, doi:10.1029/2004JA010689.
- Pallamraju, D., S. Chakrabarti, R. Doe, and T. Pedersen (2004), First ground-based OI 630 nm optical measurements of daytime cusplike and F-region auroral precipitation, *Geophys. Res. Lett.*, 31, L08807, doi:10.1029/2003GL019173.
- Rees, D., M. Conde, Å. Steen, and U. Brändström (2000), The first daytime ground-based optical image of the aurora, *Geophys. Res. Lett.*, 27, 313–316, doi:10.1029/1999GL003696.
- Remick, K. J., R. W. Smith, and D. Lummerzheim (2001), The significance of resonant scatter in the measurement of N₂⁺ first negative 0-1 emissions during auroral activity, *J. Atmos. Sol. Terr. Phys.*, 64, 295–308.
- Sandholt, P. E., H. Carlson, and A. Egeland (2002), *Dayside and Polar Cap Aurora*, Springer, New York.
- Spann, J. F., M. Brittnacher, R. Elsen, G. A. Germany, and G. K. Parks (1998), Initial response and complex polar cap structures of the aurora in response to the January 10, 1997 magnetic cloud, *Geophys. Res. Lett.*, 25, 2577–2580.
- Vallance Jones, A. (1974), *Aurora*, 301 pp., Springer, New York.
- Zhang, Y., L. J. Paxton, D. Morrison, B. Wolven, H. Kil, and S. Wing (2005), Nightside detached auroras due to precipitating protons/ions during intense magnetic storms, *J. Geophys. Res.*, 110, A02206, doi:10.1029/2004JA010498.
- Zhou, X.-Y., and B. T. Tsurutani (1999), Rapid intensification and propagation of the dayside aurora: Large scale interplanetary pressure pulses (fast shocks), *Geophys. Res. Lett.*, 26, 1097–1100.
- Zhou, X.-Y., R. J. Strangeway, P. C. Anderson, D. G. Sibeck, B. T. Tsurutani, G. Haerendel, H. U. Frey, and J. K. Arballo (2003), Shock aurora: FAST and DMSP observations, *J. Geophys. Res.*, 108(A4), 8019, doi:10.1029/2002JA009701.
- Zhou, X.-Y., D. Lummerzheim, G. R. Gladstone, S. D. Gunapala, S. B. Bandara, J. Trihne, and L. Herrell (2007), Magnetospheric application of high-altitude and long-duration balloon technology: Auroral observation under sunlight, *Adv. Space Res.*, in press.

R. Gladstone, Southwest Research Institute, 6220 Culebra Road, San Antonio, TX 78238, USA.

S. Gunapala and X.-Y. Zhou, Jet Propulsion Laboratory, 4800 Oak Grove Drive, Pasadena, CA 91109, USA. (xiaoyan.zhou@jpl.nasa.gov)

D. Lummerzheim, Geophysical Institute, University of Alaska at Fairbanks, 903 Koyukuk Drive, Fairbanks, AK 99775, USA.